8 MICROSCALE SLOW GAS FLOWS, IP METHOD

8.1 INTRODUCTION

The research on the rarefied gas flows carried out by mankind commenced at the beginning of the 20th century from the study of the low speed flows of micro scale. In the middle of the 20th century owing to the demands in the aerospace exploration the interest of the rarefied gas dynamics was concentrated mainly on the flows around bodies flying with hypersonic speed. At the end of the 20th century microscale low speed gas flows rekindled the interest of the rarefied gas dynamics community. But after near a hundred years the motivation of the study has transferred from the research on the basic problems of science into the application study related to the manufacture and the prediction of the performances of the micro-machines. There are tremendous changes in the complexity of the flow patterns and the tools of analysis of the problems.

At the beginning of the 20th century there were the experimental research of Knudsen on the mass flow rate of gas flowing through tiny tubes [1] and the experimental study by Millikan, Knudsen and Weber on the drag of small sphere in the air [2, 3, 4]. All these were important basic research topics. Knudsen obtained the result that the normalized mass flow rate through the tube had a minimum in the transitional regime (the *Knudsen paradox* or *Knudsen minimum*), Millikan measured the velocity of the charged oil drop and with the help of the formula of the low speed drag of the small sphere in the air determined exactly the electric charge of the electron (for this he won the Nobel prize in 1923).

Richard Feynman in his lecture 'There's plenty of room at the bottom' at the 1959 annual meeting of the American Institute of Physics envisaged the possibility of manufacture of micromachines by the chip processing technology, analyzed the difficulties that might encountered with the manipulation and control of micromachines, and even offered a reward of 1000 U.S. dollars for the manufacture

of a micro motor with diameter less that $1/64$ inch ($400\mu m$). The reward was won by McLellan in November 1960 for making a small motor which was rather an art work than a machine. In the late 1980s commenced the fabrication and the research of the flows in the *micro-electro-mechanical systems* (*MEMS*). By the 1990s the micromachinary fabrication techniques became mature, including the combined surface-bulk silicon micro machining, EDM (electro discharge machining) and LIGA (abbreviation of German words Lithographie Galvanoformung Abformung, i. e., lithographic electroforming) etc. The size of most tiny micro motors at present day is $1 \sim 10nm$. The *Journal of Microelectromechanical Systems* for paying deserved honor to R.P. Feynman for his farsightedness and insight republished this 1959 lecture in the Journal's initial issue [5]. (R. P. Feynman's main contribution, of course, is his fundamental research in quantum electrodynamics for which he won the physics Nobel prize in 1965)

The micro electro mechanical systems (MEMS) fabricated by these techniques are complicated systems in which simultaneously occur the motion of the working media, the perception of the sensors and the retroaction controlled by the electronic components. The full system simulation of MEMS is beyond the scope of this book: out of the three functions of MEMS only the motion of the working media is concerned. And in the following sections only the case of gas media will be addressed in detail. For the case of liquid media, as it was explained in section 6.8, the MD method is the appropriate means of simulation. The MD simulations revealed strong density fluctuation of the liquid molecules along the normal direction near the wall [6] which is the result of layered structure of the liquid molecules that have a tendency to arrange in rows parallel to the wall. The layering phenomenon of the liquid molecules near the wall is the basis of the origination of the slip boundary condition in liquid (see Thompson and Troian [7]) and the anomalous diffusion (the diffusion coefficient in the vicinity of the wall decreases or increases by a large portion in comparison with that in the bulk of the liquid). Also, in the liquid such phenomena as the wetting, adsorption and electro-kinetics (the accumulation of ions near the dielectric surfaces that can be driven by the voltage difference) closely related to the surface effects become prevailing.

To have an idea of the typical spatial and temporal sizes and the flow parameter (such as the Knudsen number etc.) ranges of the micro devices let's have a close

look at the modern Winchester hard disc drive [8, 9] and the micromachined channel fabricated both by the UCLA- CALTECH [10, 11, 12] and MIT [13, 14] groups.

In a Winchester-type hard disc drive the write/read head floats approximately $50nm$ above the spinning platter surface. The head, the platter and the gas layer between them together form a thin film slider air bearing. The characteristic length (the height) is less than the mean free path ($\sim 65nm$) of molecules in air at STP. The typical Knudsen number is about 1.3. The platter speed is typically about $25m/s$ (at radius $5cm$ of the magnetic disc rotating at 4800 revolutions per minutes), corresponding to a Mach number of ~0.07 and a Reynolds number of ~0.12 (see Eq. (0.27)). To enhance the recording capacity the gap is expected to further decrease resulting in a further increase of the Kn number, and with the increase of the revolution the Mach number and Reynolds number can also increase. The typical length of the slider bearings in disc drives is 1 mm, i. e. , 20,000 times the gap at the rear edge of the head, and the width is usually $1/10 \sim 1/3$ of the length.

The UCLA- CALTECH group first proposed and fabricated an integrated micro-channel/pressure sensor system using the combined surface-bulk silicon micro-machining. The microchannels are formed by silicon with a $1.2\mu m$ layer of wet oxide on the silicon substrate then bulk-etched with HF to obtain a channel with straight vertical walls of a height of $1.2\mu m$. Surface micromachining also enables them to make micro sized pressure sensors integrated with the flow system. The second generation micro channel is $40\mu m$ wide and $1.2\mu m$ high with 11 pressure sensors uniformly distributed along $4000\mu m$ length of the channel with intervals of $400\mu m$, the reading from the other two end sensors are omitted for the end effects. Both helium and nitrogen are used as working media. When nitrogen is used, as the mean free path of nitrogen molecules is almost the same as that of the air, the Knudsen number at the outlet of the channel under STP is ~0.055, but when helium is used, as the mean free path is inversely proportional to the squire root of the molecular mass (see Eq. (2.222)), the Knudsen number is ~0.16, the flow is surely beyond the slip flow regime. Reference [12] showed that under the conditions of the experiment the Reynolds number is less than 0.07 for nitrogen and less than 0.009 for helium, corresponding to Mach number of

~0.0026 and 0.00089 respectively. The MIT micro channel is fabricated approximately the same way with a height of 1.33, width of 52.25 and length of $7500\mu m$. To measure exactly the flow rate the modified accumulation techniques have been developed and the thermal stability requirements have been decreased by five orders of magnitude [13,14]. Nitrogen, argon, carbon dioxide and helium have been used, the flow of argon has a Knudsen number of 0.05 at the exit at an atmospheric pressure, that of helium has a $Kn \sim 2.5$ at the exit at a low pressure of $6.5 \times 10^3 Pa$.

The silicon micromachining fabrication technology has manufactured besides micro channels also micro nozzles, micro valves, micro accelerometers, micro pumps, micro motors and other micro devices. The gas flows in them owing to the micro scale of the devices usually enter into the slip flow regime, and the flows in micro channel, micro pump, micro valve, micro nozzle and the hard disc drive slider bearing enter the transitional flow regime. Thus for simulation of the gas flows in MEMS the methods of molecular gas dynamics or rarefied gas dynamics must be invoked. The objects of study in comparison with circular pipes and sphere studied in the beginning of 20th century are much more complicated. As for the tools of solution various methods developed in the transitional regime and elucidated in chapter 6 can be utilized. In MEMS the flow is usually very slow, the information to noise ratio is very small, thus leads to difficulties in statistical simulation. In the next section some methods of solution of the rarefied flow problems, such as the method of linearized Boltzmann equation, the Lattice Boltzmann method (LBM), the slip Navier-Stokes solution and the direct simulation Monte Carlo (DSMC) method, will be examined from the point of view of utilization for simulation of the flows in MEMS. In particular the unfeasibility of LBM in simulation of transitional flow is shown by comparison with the DSMC results. A method developed by Fan and Shen called the information preservation (IP) method allows the simulated molecules to carry the macroscopic information of the enormous number of molecules one simulated molecule represents, uses it to obtain the macroscopic characteristics, and in principle has found the way to overcome difficulties of large noisy to useful information ratio. The IP method will be introduced in section 8.3, with a general description and some validation of the method and a program demonstrating the method. In section 8.4 the results of

IP simulation for the unidirectional flows are described. The specific features of low flow speed and large length to height ratio of flows in MEMS pose a problem of elliptic nature with boundary conditions set far apart and requiring to be specified in the process of solution, leading to the issue of mutual influence of the inlet and outlet boundary conditions and the need to regulate them. The resolving of the boundary condition regulation problem by using the conservative scheme of continuity equation and the super relaxation method is illustrated on the example of flow in long micro channels in section 8.5. The thin film air bearing problem is solved in section 8.6. By using the same scheme and method the IP simulation of the flow of authentic length of the hard disc drive is described and compared with the result of the Reynolds equation. The use of the degenerated Reynolds equation is suggested by the author to solve the microchannel flow and to serve as a criterion with the merit of strict kinetic theory to test various methods intending to solve the transitional internal MEMS flows. The method, the comparison with the experimental data and the IP calculation and the test of the LBM by it is given in section 8.7. Finally, some review and summary are given in section 8.8.

8.2 METHODS FOR SOLVING THE RAREFIED GAS FLOWS IN MEMS

In the previous section we have seen that the gas flows in MEMS typically are in the slip and transitional flow regimes. The method of Navier-Stokes equation plus slip boundary condition, the method of linearized Boltzmann equation, the Lattice Boltzmann method and the direct simulation Monte Carlo (DSMC) method will be examined in this section from the point of view of utilization for simulation the flows in MEMS.

The solution of the rarefied gas dynamics problems by using the *Navier-Stokes equation with slip boundary conditions* (see Chapter 5) can make advantage of the mature and efficient methods of the Computational Fluid Dynamics (CFD). Karniadakis and Sherwin developed high order finite element (spectra element) method [15] to solve the compressible and incompressible Navier-Stokes equations with the first and higher order slip boundary condition, and by using the so called μ Flow code solved many interesting MEMS flow problems which

were also reported in [16]. There is no doubt about the appropriateness of this method in solving problem in the slip flow regime. Kardiadakis and Beskok extended the method for use in micro flows with Kn as high as 0.5. This seems to be a kind of extrapolation beyond the reasonable application range. But it brings into full play the high efficiency of the continuum model in treating the complex geometries. Still one should be cautious relative to the results of the extrapolation. Here we cite two examples with one showing the necessity of the caution and the other showing the success of the extrapolation. The first example is the calculation of mass flow rates through short micro channels [17]. The flow rates obtained by the Navier-Stokes equation with slip boundary conditions and the DSMC methods (see Fig. 8.1) differs significantly as $Kn > 0.1$, and the slip Navier-Stokes solution can not yield the flux minimum predicted first by Knudsen [1] experimentally (for more detailed account of the Knudsen minimum see section 8.4). The second example is the flow in the air bearing between the read/write head and the hard disc drive platter. The slip corrected Reynolds equation can provide result in fair agreement with the DSMC result for Knudsen number as high as 4.2 (see [18]). But the calculation by the generalized Reynolds equation based on the solution of the linearized Boltzmann equation for the flow rate of Poiseulille flow by Fukui and Kaneko [19] is in excellent agreement with the result of DSMC. This latter success of course must attribute to the employment of the Boltzmann equation that

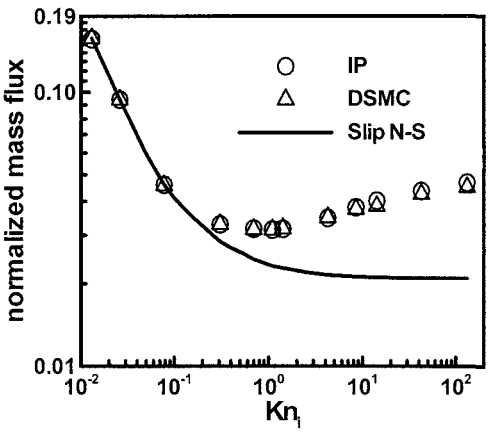

Fig. 8.1 The variation of the mass flux through short channels calculated by the IP, DSMC methods and the Navier-Stokes equation with slip boundary conditions [17]

is appropriate in the entire transitional regime. (For more detailed account of the thin film air bearing problem see section 8.6.)

The linearized Boltzmann equation (see section 6.2) is suitable for solution of low speed problems in MEMS, and can serve as the criterion for testing other methods. At the same time the linearized Boltzmann equation can be used to solve the flow field with temperature variation which is the typical case in MEMS. It is an actual task to develop the solution of the linearized Boltzmann equation to complex geometry. Some times the equation being linearized is not the Boltzmann equation but the BGK equation, in which case the solution is much simpler. But to make the solution of the BGK equation corresponding to the physical reality, some modification of the kind of parameter regulation is needed. And there are still differences between such solution and the solution based on real molecule models.

At the second half of 1980 years Frish et al. developed *the lattice gas method* [20], in which particles are allocated at lattice consisting of equilateral triangles with velocities either along the sides of the triangles or equal zero. Every time step the particles move a cell length (except the particles with zero velocity), and it is shown that Navier –Stoke equation can be obtained from such lattice gas. The shortcomings of such lattice gas are: the amount of work increases with the increase of Reynolds number, and it can only simulate incompressible fluid under small Mach number and the statistical noise is large. The first two shortcomings are tolerable for small speed micro flows. The latter shortcoming is essential and is resolved by introducing the *lattice Bolotzmann method* (LBM, see [21] and [22], and the literature cited in the latter). Lattice Boltzmann method integrates the kinetic theory equation (Boltzmann equation or its simplified version) at the location of each lattice along each discrete velocity. The arithmetic operations of this method are simple, and it is easy to treat arbitrary complex geometry and implement parallel computation. It seems especially suitable for treating micro scale flows. Recently Nie, Doolen and Chen [23] simulated the flows in microchannels under large Knudsen numbers in the transitional regime using the LBM and obtained results of the pressure distribution etc. The microchannel flows under the same parameters are simulated in [24, 25] using both Nie et al.'s LBM method and DSMC method to examine the feasibility of the LBM method in the transitional

regime. The simulation results show that for small Knudsen number ($Kn = 0.0194$) the LBM and DSMC methods agree fairly well. For $Kn = 0.194$, the velocity profiles of the LBM and the DSMC (as well the IP) methods differ slightly, but the pressure distribution results have apparent difference (see Fig. 8.2). In the transitional regime, when $Kn = 0.388$, the DSMC simulation results do not verify the negative deviation of the pressure from the linear distribution predicted by the LBM method, and the results of the LBM and DSMC differ significantly in magnitudes (see Fig. 8.3). This shows clearly that this version of LBM is not able to simulate the MEMS flows in transitional regime.

The direct simulation Monte Carlo (DSMC) method (see Chapter 7) is an appropriate method to treat gas flows in MEMS and is able to simulate flow problems in regimes from free molecular to continuum. The simulation results of DSMC for bench mark problems can be used as criteria for other methods and it is able to treat problems abundant physical contents, including chemical vapor deposition, plasma processing and the flow field with temperature variations. But utilization of DSMC method in MEMS flows encounters with the problems of the excessively high demands to the storage and computation time of the computer. Take the micro channels with embedded pressure sensors fabricated by the global processing techniques [10, 11] as example, the size being $1.2 \times 40 \times 3000 \mu m^3$.

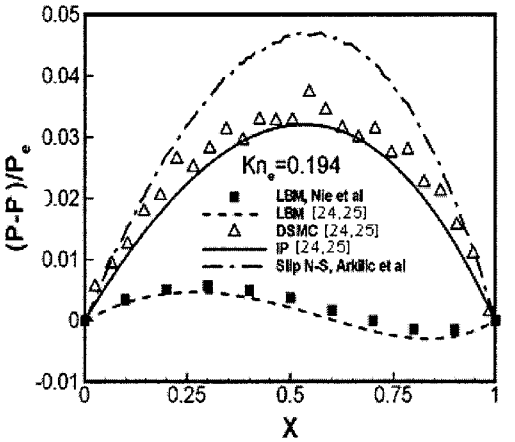

Fig. 8.2 Comparison of the deviation of the stream-wise pressure from a linear pressure distribution given by LBM, DSMC, IP, and slip Navier-Stokes equation, for the case of $Kn = 0.194$ [24,25]

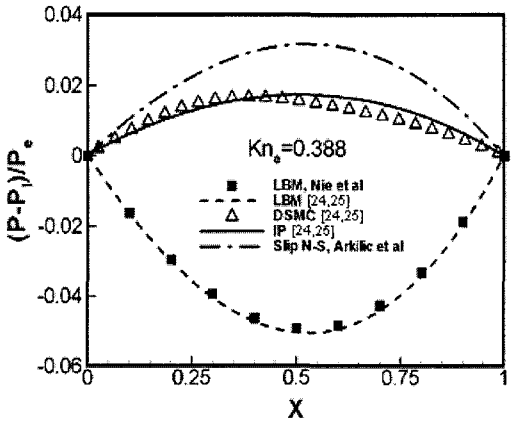

Fig. 8.3 Comparison of the deviation of the stream-wise pressure from a linear pressure distribution given by LBM, DSMC, IP, and slip Navier-Stokes equation, for the case of $Kn = 0.388$ [24,25]

When the cell dimension Δr is taken of the order of the mean free path λ, even treating the problem as two-dimensional (neglect the span wise variation), 6×10^5 cells must be allocated. If distribute 20 molecules in each cell, about 10^7 molecules must be followed in the simulation. The macroscopic velocity of the gas flow in the experiments of [10-14] is $0.2\sim0.5m/s$, the time for transiting the channel is about $10^{-2}s$, or $10^8\Delta t$ (the time step Δt is taken as the order of the collision time $10^{-10}s$). This makes un-accomplishable the task of gradual regulating the inlet and outlet boundary conditions of the channel to gain the steadiness of the flow (this requires multiple transit times). The difficulty of simulating the low speed flow in MEMS also lies in huge statistical scatter on the DSMC results. The order of the useful information is of the order $U = 0.2m/s$, and the background noise under room temperature $c_m = \sqrt{2kT/m}$ is of the order of $10^3 m/s$. Only when the sample size N is as big as 10^8, the standard deviation $c_m/\sqrt{N}$ could be small enough, and this is an excessive requirement for the computation time. This makes some researchers think that DSMC is not suitable for simulating gas flows inside MEMS [26]. In fact there have been many experimental results of the micro-channel flows [10-14], at the same time the DSMC simulation of the micro channel flow has been limited to the high speed and even hypersonic cases [27, 28].

Recently the results of the DSMC method with fluctuations have been filtered by using the flux-corrected transport (FCT) method [29] as filter. It is shown, that when the flow velocities are much smaller than the thermal velocity and the number of the real molecules is much larger than the number of simulated molecules, FCT can extract smooth solution from the noisy solution of DSMC with the high frequency statistical fluctuations eliminated. But verification by experiment or exact solution is needed to judge whether the filtered solution is in exact agreement with physically real solution.

8.3 INFORMATION PRESERVATION (IP) METHOD

8.3.1 THE DESCRIPTION OF THE METHOD

Fan and Shen proposed a particle-based method, called the *information preservation (IP) method* [30, 31], to treat the problems encountered by the DSMC method of the huge ratio of the noise to the useful information and the demand of extremely large sample size. This is a method imbedded in the DSMC method in which each simulated molecule is assigned two velocities: thermal velocity $\boldsymbol{c}$ and information velocity $\boldsymbol{u}_i$. The former is just the molecular velocity $\boldsymbol{c}$ in the DSMC method and is used to calculate the motion, collision and the reflection of molecules at the surfaces following the same algorithms and models as the DSMC method. Besides $\boldsymbol{c}$ we suppose that each molecule carries the so called *information velocity (IP velocity)* $\boldsymbol{u}_i$ to record the collective velocity of the enormous number of real molecules represented by each simulated molecule. The IP velocities do not produce any influence on the motion of molecules, and are used only for summation to obtain the macroscopic velocities, the primitive information is taken from the oncoming flow and the body surface. When the molecules reflect from the surface, collide with each other, experience force action and enter from boundary, the IP velocities attain new values [30-33, 17]:

1. For simulated molecules diffusely reflected from a wall, the reflected IP velocity $\boldsymbol{u}_i$ has the same velocity as the wall. If the wall has a tangential momentum accommodation coefficient of value σ the reflected molecule with a probabil-

ity of σ has an IP velocity the same as the wall, and with a probability $(1-\sigma)$ retains its tangential velocity before incidence.

2. For two simulated molecules colliding each other, the post-collision IP velocities satisfy the momentum conservation

$$u_{i,1}^{*} = u_{i,2}^{*} = \frac{m_1 u_{i,1} + m_2 u_{i,2}}{m_1 + m_2}, \tag{8. 1}$$

where superscript * denotes post-collision quantities.

3. If there are external forces acting on a cell, acceleration $\boldsymbol{a} = \boldsymbol{F}/\rho\Delta V$ will contribute an velocity increment $\boldsymbol{a}\Delta V$ to each simulated molecule during a time step Δt, where $\boldsymbol{F}$ is the sum of the external forces, ρ and ΔV are the density and volume of the cell, respectively.
4. For simulated molecules entering the computational domain from boundaries, $\boldsymbol{u}_i$ is set to satisfy the boundary condition.
5. In general under the isothermal assumption (which is valid for slow subsonic micro flows without heating) the IP velocity $\boldsymbol{u}_i$ of the simulated molecule and the IP velocity $\boldsymbol{U}$ and IP density ρ (or n) of the cell are introduced which obey the mass conservation and momentum conservation equations

$$\iiint \frac{\partial \rho}{\partial t} dV = \iint \rho \boldsymbol{U} \cdot \boldsymbol{l} dS, \tag{8.2}$$

$$\iiint \rho \frac{d\boldsymbol{U}}{dt} dV = -\iint p \boldsymbol{l} dS, \tag{8.3}$$

where the integrals are taken on the volume and surfaces of a cell, $\boldsymbol{l}$ is the external normal vector of the surface. It is noted that in the right hand side of the momentum equation only a non-viscous term is retained. In fact the IP quantities are governed by a general momentum equation

$$\iiint \rho \frac{d\boldsymbol{U}}{dt} dV = -\iint \boldsymbol{\sigma} \boldsymbol{l} dS \equiv -\iint p \boldsymbol{l} dS + \iint \boldsymbol{\tau} \boldsymbol{l} dS, \tag{8.4}$$

where $\boldsymbol{\sigma}$ is the pressure stress tensor and $\boldsymbol{\tau}$ is the viscous stress tensor. But as the IP quantities are carried along by the simulated molecules of the DSMC process which migrate across the cell surface in the positive and negative direction and

implement the action of viscous transport, so although the IP quantities are written formally as governed by an inviscid momentum equation, but as the IP process is embedded in the DSMC process, the IP quantities are factually governed by a more complete conservation law including the viscous transport. After a time step Δt the cell IP density attains increment according to Eq. (8.2)

$$\Delta\rho = -\frac{\Delta t}{\Delta V}\iint \rho \boldsymbol{U}\cdot \boldsymbol{l}dS\,, \tag{8.5}$$

from where the density and pressure are also renewed : $p = nkT$. The increment of the IP velocity of the cell is, according to Eq. (8.3),

$$\Delta \boldsymbol{u} = -\frac{\Delta t}{\rho \Delta V}\iint p\boldsymbol{l}dS\,, \tag{8.6}$$

and is added to the IP velocity of the simulated molecules in the cell. The renewed quantities are used for the next step calculation. This step of the renewal of the IP quantities is conducted after 'calculation of collisions corresponding to time Δt' (see Fig.7.2 Flow Chart of program of the DSMC-IP method). The calculation of the macroscopic quantities should employ the information velocities introduced, for example, the macroscopic velocity of a cell is obtained from the averaging of the IP velocities of molecules in the cell

$$u_0 = \frac{1}{N_c}\sum_{k=1}^{N_c} u_{i,k} \tag{8.7}$$

where N_c is the number of simulated molecules in the cell; k is the index of the molecules in a cell. The shear stress on a surface element with area ΔA_w is given by

$$\tau_w = \frac{\sum_{j=1}^{N_t} m(u_{t,j}^{i} - u_{t,j}^{r})}{t_s \Delta A_w} \tag{8.8}$$

where N_t is the total number of molecules incident to the element during the sampling time t_s, subscript t denotes the tangential direction of the element, and superscripts i and r denote the incident and reflecting values of the IP velocities, respectively.

8.3.2 THE VALIDATION OF THE METHOD

Now we validate the reflection rule of the IP procedure [34]. For simplicity we validate the case of diffuse reflection, namely, the statement 'for simulated molecules diffusely reflected from a wall, the reflected IP velocity $\boldsymbol{u}_i$ has the same velocity as the wall' in step 1). The extension to the case of incomplete diffuse reflection does not pose any principle difficulty. As a simulated molecule represents an enormous number of real molecules, we trace the velocities of the numerous real reflected molecules and obtain the IP value by averaging. An individual molecule after *diffuse reflection from a stationary surface* would have velocity with the components

$$u = -(\ln(ranf))^{1/2} / \beta \,, \tag{8.9}$$

$$v = V \cos\theta \,, \tag{8.10}$$

$$w = V \sin\theta \,, \tag{8.11}$$

where

$$\beta = (2\frac{k}{m}T_w)^{-1/2} \,, \tag{8.12}$$

$$V = -(\ln(ranf))^{1/2} / \beta \,, \tag{8.13}$$

$$\theta = 2\pi ranf \,, \tag{8.14}$$

and $ranf$ is a random fraction uniformly distributed between 0 and 1 (see Eqs (3.20), (3.15), (3.12), (3.18) and (3.19) of section 3.2). In the DSMC procedure one records these individual components (with concrete values of $ranf$) and then uses them to obtain the macroscopic quantities only in the step 'sampling of the flow properties'. In the IP procedure we record the averaged values of u , v and w already at this stage of reflection. From the derivation of Eq. (3.20) (Eq. (8.9)) and the practice of the DSMC procedure, one sees that thus sampled velocity components u in the whole guarantees the correct value of the mass flux of dif-

fusely reflected molecules and yields no macroscopic velocity in the normal to surface direction. So after averaging all u, the zero macroscopic velocity component is obtained:

$$\bar{u} = 0 . \tag{8.15}$$

The averaging of v yields:

$$\bar{v} = \overline{V\cos\theta} = \bar{V}\overline{\cos\theta} = 0 , \tag{8.16}$$

as v and $\cos\theta$ are independent variates and

$$\overline{\cos\theta} = 0$$

according to Eq. (8.14). Similarly one has

$$\bar{w} = 0 . \tag{8.17}$$

If the surface is not stationary but has certain velocity, the velocity components would have been added to u, v, w, and after averaging this velocity would be obtained as the IP velocity after diffuse reflection. So the statement 'for simulated molecules diffusely reflected from a wall, the reflected IP velocity $\boldsymbol{u}_i$ has the same velocity as the wall' is verified.

Next we validate the collision rule of the IP procedure [34, 35]. The components of the post-collision velocities of the two collision partners (with velocity components u_1, v_1, w_1 and u_2, v_2, w_2 before collision) have been found already in section 2.4.5 (see Eq. (2.112)):

$$\begin{aligned}
u_1^* &= \frac{m_1u_1 + m_2u_2}{m_1 + m_2} + \frac{m_2}{m_1 + m_2}\sin\theta\cos\phi c_r^*, \\
u_2^* &= \frac{m_1u_1 + m_2u_2}{m_1 + m_2} - \frac{m_1}{m_1 + m_2}\sin\theta\cos\phi c_r^*, \\
v_1^* &= \frac{m_1v_1 + m_2v_2}{m_1 + m_2} + \frac{m_2}{m_1 + m_2}\sin\theta\sin\phi c_r^*, \\
v_2^* &= \frac{m_1v_1 + m_2v_2}{m_1 + m_2} - \frac{m_1}{m_1 + m_2}\sin\theta\sin\phi c_r^*, \\
w_1^* &= \frac{m_1w_1 + m_2w_2}{m_1 + m_2} + \frac{m_2}{m_1 + m_2}\cos\theta c_r^*, \\
w_2^* &= \frac{m_1w_1 + m_2w_2}{m_1 + m_2} - \frac{m_1}{m_1 + m_2}\cos\theta c_r^*.
\end{aligned} \tag{8.18}$$

where ϕ is a variate uniformly distributed between 0 and 2π, and $\cos\theta$ is a variate uniformly distributed between -1 and 1. Here we understand $u_1, v_1, w_1, u_2, v_2, w_2$ as one set of the velocity components of many individual real molecules the two colliding simulated molecule represent. In the IP procedure we are not interested in recording the individual $u_1^*, v_1^*, w_1^*, u_2^*, v_2^*, w_2^*$ but are intending to record (preserve) the averages of velocity components of the enormous number of molecules. For example, we have from the first equation of Eqs. (8.18)

$$\begin{aligned}\overline{u_1^*} &= \overline{\frac{m_1u_1 + m_2u_2}{m_1 + m_2}} + \frac{m_2}{m_1 + m_2}\overline{\sin\theta\cos\phi c_r^*} \\ &= \frac{m_1\overline{u_1} + m_2\overline{u_2}}{m_1 + m_2} + \frac{m_2}{m_1 + m_2}\overline{\sin\theta\cos\phi}\,\overline{c_r^*} \\ &= \frac{m_1\overline{u_1} + m_2\overline{u_2}}{m_1 + m_2},\end{aligned} \tag{8.19}$$

as the $\sin\theta$ and $\cos\phi$ are independent variates and ϕ is uniformly distributed between 0 and 2π. Analogously we have

$$\overline{u_2^*} = \overline{u_1^*} = \frac{m_1\overline{u_1} + m_2\overline{u_2}}{m_1 + m_2}, \tag{8.20}$$

$$\overline{v_1^*} = \overline{v_2^*} = \frac{m_1\overline{v_1} + m_2\overline{v_2}}{m_1 + m_2}, \tag{8.21}$$

$$\overline{w_2^*} = \overline{w_1^*} = \frac{m_1\overline{w_1} + m_2\overline{w_2}}{m_1 + m_2}. \tag{8.22}$$

Thus, the IP collision rule, Eq. (8.1) of step 2), has been validated. As the IP procedure uses the already averaged values to obtain the macroscopic quantities (see Eq. (8.7)), it is natural that the sample size needed for convergent IP averaging is much less than that needed in the DSMC procedure.

8.3.3 PROGRAM DEMONSTRATING THE METHOD

In section 7.3 a FORTRAN program is given to demonstrate the solution of Couette problem by the DSMC method (see Appendix IV), it is also used to demonstrate the IP method. In this program VMEAN(I, NO-MOLECULE), $I = 1,2,3$, are introduced to denote IP velocities. The statements in the program used to implement the changes in the IP method are marked with * and **, the statement marked with * signify that it is used to replace the statement before it, those statements marked with ** signify that they are the statements needed to be added anew. The above described cases of changes of the IP velocities and the procedure of obtaining the macroscopic quantities from the IP velocities are shown in the program (see section 7.3 and the statements in the program in Appendix IV marked with * and **).

When employing the IP method, another change should be introduced as well. This is the change in the collision cross sections of the molecules. In section 2.4 the expression of viscosity coefficient μ for various molecular models has been given according to the Chapman-Enskog transport theory in the kinetic theory (see Eq. (2.71)), and the diameters of molecules have been determined (for HS model, see Eq. (2.77), for VHS and VSS models, see Eq. (2.234), where the reference diameter of molecules is given by Eq. (2.235)). In the IP method, when assigning the IP velocities after collision, we stipulate they follow the macroscopic momentum conservation law, Eq. (8.1), but in the DSMC method the velocities after collision are assigned according to the momentum conservation in each collision (the detailed conservation), and this is the condition implied in obtaining the expressions of d for various models. The difference in the assignment of the post –collision velocities leads to the necessity of modification of the collision cross section in the IP method to obtain the correct value of viscosity μ. The concrete method is to obtain the correct experimental value of μ by varying d, in employing the IP method to solve the Couette problem under small Kn number (see [31]). Take the HS model as example. The collision diameter (see Eq. (2.77))

$$d_{HS} = \left(\frac{5mc_m}{16\sqrt{2\pi}\mu}\right)^{1/2}, \tag{8.23}$$

is used as the initial value of the collision diameter in the IP method, the shear stress τ_{xy} of each cell can be calculated according a formula analogous to Eq. (8.8), from where the value of μ, $\mu = \tau_{xy}\Delta y / \Delta u$, of the cell is obtained, the viscosity μ is obtained as the average of the μ values in various cells (except the cells in the Knudsen layer). The diameter of HS model is modified according to the difference between this value and the experimental μ value (the increase of d_{HS} makes μ decreasing), until the correct experimental μ value is obtained. The d_{HS} thus fixed is the value to be used in the IP method. The reference diameters of the VHS model can be obtained by analogous method [31]. Some values of d_{HS} and reference diameters d_{ref} of the VHS model are listed in Table 3 of Appendix I. In the example program demonstrating the IP method, the collision diameter of the Ar molecule, when employing the IP method , is replaced by $d_{HS} = 3.963 \times 10^{-10} m$ (see the first statement with * in subroutine subc1 in the program).

8.4 UNIDIRECTIONAL FLOWS

The Couette flow is a steady flow of gas occurred between two parallel plates moving with velocity U_w in opposite directions along their own planes. The velocity profiles and the shear stress profile obtained by using the IP method in simulating the Couette flow [30, 31] are given in Fig. 8.4 and Fig. 8.5. The velocity profiles are given under three Knudsen numbers, $Kn = 0.1128$, $Kn = 1.128$ and $Kn = 11.28$, and are compared with the solutions of the linearized Boltzmann equation [36], of the moment method [37] and of the Navier-Stokes equation plus the slip boundary condition (see section 5.4.1, Eq. (5.65)). The velocity profiles of the IP method under the small, medium and large Kn numbers are all in good agreement with the solution of the linearized Boltzmann equation of Sone et al., but the agreement between the moment method of the second order approximation by Gross and Ziering and the result of the linearized Boltzmann equation (and the IP method) is not so good, especially for medium Knudsen number. The solution of the Navier-Stokes equation plus the slip boundary condition yields relatively

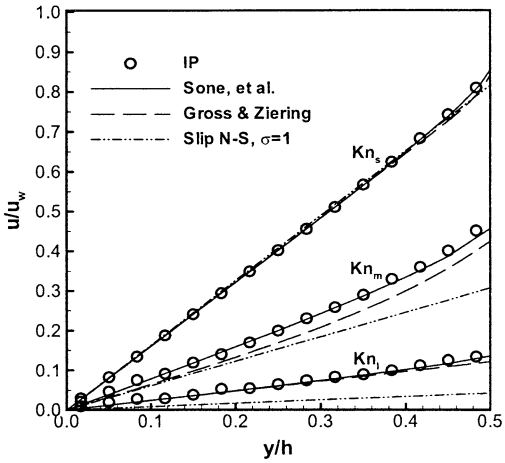

Fig. 8.4 Velocity profiles of the Couette flow for $Kn_s = 0.1128$, $Kn_m = 1.128$ and $Kn_l = 11.28$. Comparison of the IP method [30], the linearized Boltzmann equation [36], the moment method [37] and the Navier-Stokes equation plus slip boundary condition

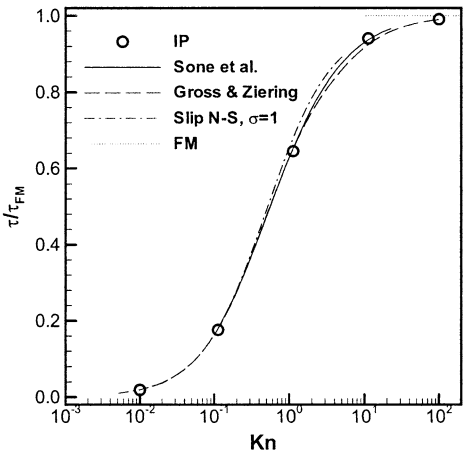

Fig. 8.5 Variation of the shear stress with Kn in the Couette flow. Comparison of the IP method [30], the linearized Boltzmann equation [36], the moment method [37], the Navier-Stokes equation plus slip boundary condition and the free molecular flow theory

good result only for small Knudsen numbers. The shear stress in the Couette problem solved by the Navier-Stokes plus slip boundary condition (see Eq. (5.64) in Chapter 5) is a case incidentally appropriate for the entire transitional regime. The solutions of the IP method, of the linearized Boltzmann equation, of the moment method and of the Navier-Stokes equation plus slip boundary condition are in good agreement in the whole transitional regime (see Fig. 8.5, in which $\tau_{FM} = \rho c_m U_w / \sqrt{\pi}$, see Eq. (4.54), note, the wall velocity U_w here constitutes only half of the velocity U in section 4. 5). It is noted that the IP method is in exact agreement with the solution of the linearized Boltzmann equation, and simultaneously agrees with the theoretical solution of the free molecular flow in the collisionless limit.

In section 7.3 it has been mentioned that the DSMC program aimed at the Couette flow problem can be amended to be used in solving the Poiseuille flow and the Rayleigh problem, the same is true for the IP method. The results of solution of the planar Poiseuille flow and the Rayleigh problem by the IP method were presented in detail in [30, 31], here only the mass flow rate of the Poiseuille flow and the velocity profile and the shear stress in the Raylegh problem will be discussed.

The mass flow rate of the Poiseuille flow has been calculated by the Navier-Stokes equation with slip condition on the boundary in section 5.4.2 (see Eq. (5.74)). This $Q_{P,SL}$ is a monotonically descending function of Kn. But at the beginning of the 20th century Knudsen [1] discovered through experiments that there appears a minimum of the mass flow rate in transitional regime, this is the so called *Knudsen minimum* or the *Knudsen paradox.* This result was confirmed in the later experiments [38] for many gases (air, helium, hydrogen, carbon dioxide and Freon-12). Fig. 8.6 shows the comparison of various methods and the experiment ($u^* = \alpha c_m$, α is a pressure gradient factor, see Eq. (7.11)). The result of the IP method agrees with Eq. (5.74) (for $\sigma = 1$) under small Kn numbers, yields the Knudsen minimum under medium Kn numbers and agrees with the numerical solution of the linearized Boltzmann equation [39] and the experimental data, demonstrating the ability of the IP method in predicting the fine flow characteristics in the transitional regime.

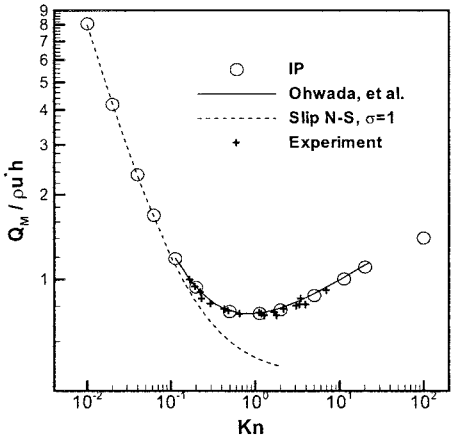

Fig. 8.6 The variation of the dimensionless mass flux in the Poiseuille flow with Kn number (comparison of IP [30] and linearized Boltzmann equation [39] with the experimental data [38].)

The velocity profiles in the Rayleigh problem obtained by the IP method in the initial stage of motion $t = 0.01\tau_c$ (τ_c collision time) agrees well with the result of free molecular flow (see Eq. (4.99) in Chapter 4), and after many collision times ($t = 100\tau_c$) agrees well with the solution of the slip Navier-Stokes equation (Eq. (5.88) in Chapter 5) (for detailed account see [30, 31]). In the transitional regime $t = 5\tau_c$, as there is no numerical solution of the Rayleigh problem by the linearized Boltzmann equation, the calculation by the DSMC method has to be employed to check the result of the IP method (see Fig. 8.7)). From the comparison it is seen that the agreement is excellent. But for the case of $U_w = 1m/s$, the DSMC method has to employ enormous sampling size 2×10^8 to reduce the statistical scatter, in the result the computational time spent is 3×10^4 times of the IP method. In Fig. 8.8 the comparison of the results of various methods of the shear stress (normalized by the value in free molecular flow $\tau_{FM} = \rho c_m U_w / 2\sqrt{\pi}$, see Eq. (4.101)) of the Rayleigh problem is given. Except the results of the IP method, the DSMC method [31], the slip Navier-Stokes equation and the FM theory, also shown is the result of the moment method [40]. The agreement of the IP method with the collisionless solution in the free molecular flow limit ($t \ll \tau_c$), with the

DSMC result in the transitional regime ($t \sim \tau_c$) and with the Navier-Stokes slip solution in the slip flow regime ($t \gg \tau_c$) is uniformly good.

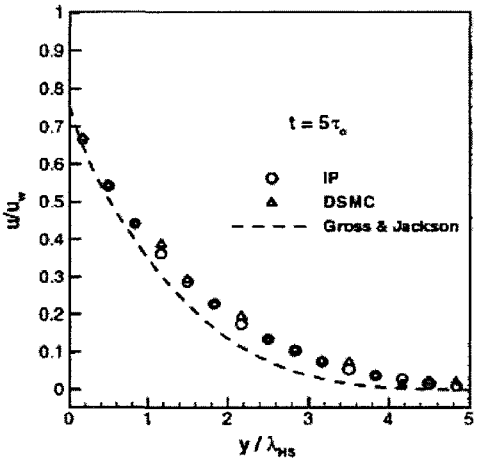

Fig. 8.7 The velocity profiles in the Rayleigh problem at $t = 5\tau_c$ obtained by the IP method, the DSMC method [30, 31] and the moment method [40]. The sample size of the IP method is 6×10^3, of the DSMC method is 2×10^8

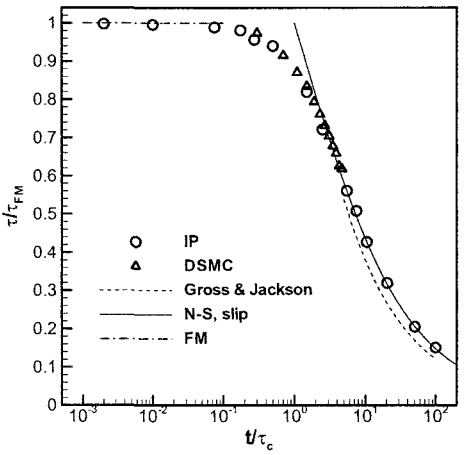

Fig. 8.8 The variation of the shear stress (normalized by $\tau_{FM} = \rho c_m U_w / 2\sqrt{\pi}$) of the Rayleigh problem with Kn number

8.5 THE MICROCHANNEL FLOW PROBLEM

In treating the unidirectional motions utilization of the steps 1), 2), 3) and 4) given in section 8.3 was sufficient for renewal of the IP velocities. Only when treat the Poiseuille flow the expression of the IP velocity increment (Eq. (8.6) of step 5) was used. When the pressure variation is expressed as

$$p = p_0(1 + \alpha x / h) , \tag{8.24}$$

the velocity increment can be found from Eq. (8.6) as

$$\Delta u = -(\alpha p_0 / \rho h)\Delta t . \tag{8.25}$$

In fact, Eq. (7.11) in section 7.3 has been obtained in this way. In the two-dimensional and three-dimensional cases the method of renewal of the cell IP velocities $\boldsymbol{U}$, the IP density ρ and the molecular IP velocities $\boldsymbol{u}$ described in step 5) should be used systematically.

Various two-dimensional problems have been solved by the IP method, including the microchannel flow [41, 42 , 43, 17], the flow around the plane plate [44, 45, 47], the flow around the airfoil [46, 48], the cavity flow [49], non-circular Poiseuille flow [50], the flow in membrane filter [51], etc.

Microchannel is the basic constituent of the MEMS devices, the geometric form is regular and simple (see Fig. 8.9), but can reveal the specific features of the low speed micro internal flows, i. e., the issue of the mutual influence of the boundary conditions at the inlet and the outlet caused by the elliptic nature of the problem. For the DSMC-IP procedure it is necessary to prescribe the values of the pressure p and the velocity distribution $\boldsymbol{U}$ over the cross sections at the inlet and the outlet of the channel to start any simulation. But fixing all p and $\boldsymbol{U}$ at the inlet and the outlet simultaneously would over determine the boundary conditions: The arbitrarily chosen p and $\boldsymbol{U}$ would be contradictory to each other. The correct values of p and $\boldsymbol{U}$ at inlet and outlet must be obtained in the process of solution of the problem. A method of fixing p as the same of the prescribed (experimental) condition and allowing $\boldsymbol{U}$ change continuously and finally reach the steady solution is adopted here [41]. Thus the process of the DSMC-IP solution is always one of gradual adjustment towards a steady state. It is very critical that the conservative form of the mass conservation equation must be employed

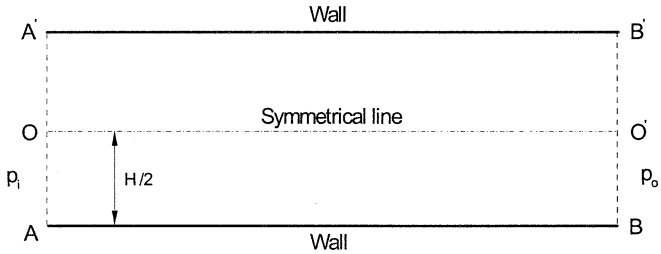

Fig. 89 Computational domain of gas flow in a microchannel

$$\frac{\partial \rho}{\partial t}+\frac{\partial \rho U}{\partial x}+\frac{\partial \rho V}{\partial y}=0\,, \tag{8.26}$$

its second order central difference scheme yields the density increment

$$\Delta\rho=\Delta t\left(\frac{\rho_{i-1,j}U_{i-1,j}-\rho_{i+1,j}U_{i+1,j}}{2\Delta x}+\frac{\rho_{i,j-1}V_{i,j-1}-\rho_{i,j+1}V_{i,j+1}}{2\Delta y}\right). \tag{8.27}$$

This density increment expression can be obtained from the integral form mass conservation equation (8.5) directly by using an integration domain ABCD $(2\Delta x\times 2\Delta y)$ with point (i,j) in the center (see Fig. 8.10). The adoption of the conservative form of the continuum equation or the integral form of conservation equation guarantees that the mass flux flown from the adjacent domain of area ABCD will flow without any numerical error into the integral area and vice versa

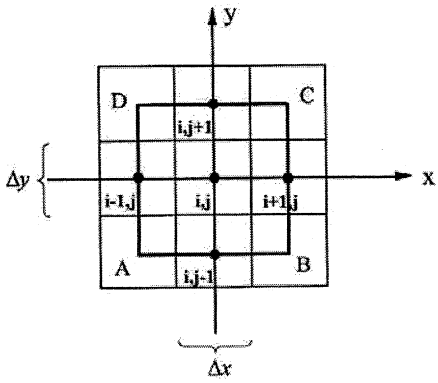

Fig. 8.10 The control surface ABCD of the conservation equation and the cell central points (i,j) in the IP method

and avoids the accumulation of numerical errors from the non-conservative scheme. This is an issue that must be taken into account whenever solving a slow rarefied channel flow or any other slow internal rarefied gas flows.

The increments $\Delta\rho$ and Δu from Eq. (8.27) and Eq. (8.6) allow one to obtain the renewed fields of ρu and ρv which are unfortunately with large fluctuations and are smoothened by a averaging technique to avoid the amplification of the errors which would influence the stability of the calculation. The increment $\Delta\rho$ obtained from Eq. (8.27) is only of the order of 10^{-9} of ρ with time step Δt being of the collision time for slow gas motion in long micro-channels [10-14]. For all simulations in such channel flows Δt has been taken as 1/2 average collision time at the inlet. Direct employment of this $\Delta\rho$ to achieve the steady (convergent) state is too time-consuming. A *super-relaxation technique* is employed to speed up the convergence process

$$\rho_{i,j}^{t+\Delta t} = \rho_{i,j}^{t} + \omega\Delta\rho_{i,j}^{t}, \tag{8.28}$$

where ω is a *super relaxation factor*. In practical calculations ω is taken to be between 100 and 2000 and trends to 1 when convergence is achieved[1].

The necessity of using the conservative form of the mass conservation is illustrated on one of the flow cases under the experimental conditions considered [12]. Helium flows through a $1.2\times40\times4000\mu m^3$ micro-channel with an inlet pressure of 19.0 psig into the atmosphere (outlet pressure 0 *psig*). Fig. 8.11 and Fig. 8.12 show the evolution of mass fluxes at all cross sections along the channel by the IP calculation. The slip Navier-Stokes solution is adopted as the initial pressure distribution. It is different from the real distribution since the flow is in the transitional regime. This resulted in a non-uniform mass flux distribution along the channel length at the initial stage of simulation (at $1\sim2\times10^3\Delta t$, the black triangles in Fig. 8.11 and Fig. 8.12). By using the conservative scheme, Eq. (8.27), and the super-relaxation technique, Eq. (8.28), a steady state is approached after about 2×10^5 time steps (the hollow spheres in Fig. 8.11). And the averag-

[1] For short channels and not slow flow speed, $\Delta\rho_{i,j}^{t}$ might be the same order of $\rho_{i,j}^{t}$, and an ω less than 1 is suggested to be used to stabilize the convergence process.

ing-smoothing process gives a relatively smooth and almost uniform mass flux distribution (solid line in Fig. 8.11). If the non-conservative scheme were used, the mass flux would remain non-uniform. Fig. 8.12 shows the mass flux distribution after 2×10^5 time steps (the hollow spheres, the solid line being the averaged smoothened data) by using the non-conservative form of the continuity equation. The mass fluxes at various cross sections have not been regulated by the simula-

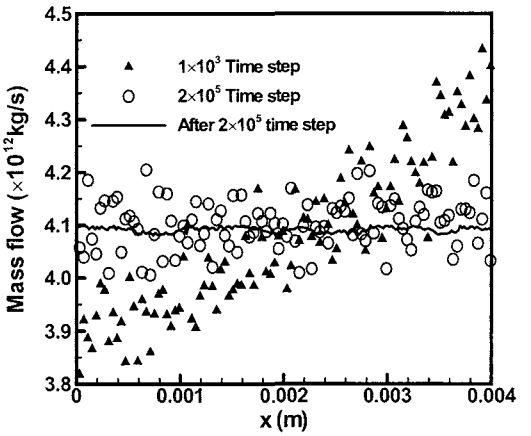

Fig. 8.11 Evolution of mass flux distribution in IP simulation of the micro-channel gas flow of [12], while the conservative form of the mass conservation equation is used

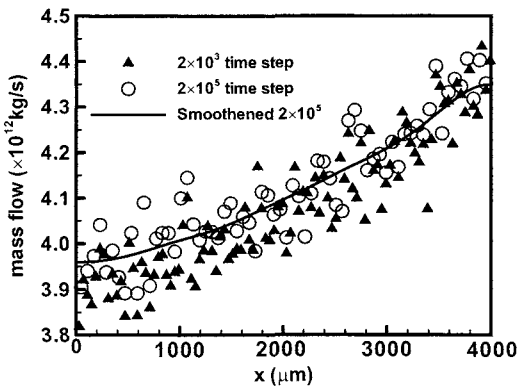

Fig. 8.12 Evolution of mass flux distribution in IP simulation of the micro-channel gas flow of [12], while a non-conservative form of the mass conservation equation is used

tion relaxation process, for the adjusting act of the mutual influence of the inlet and outlet boundaries have been damped by the numerical errors inherent in the non-conservative scheme.

The effect of the acceleration action of the super-relaxation technique is illustrated on another experimental case [11] of nitrogen flowing in a $1.2\times30\times3000\mu m^3$ channel with inlet pressure of $15psig$ into the atmosphere. Figure 8.13 shows the evolution of the density ρ at the center of the cross section located at $2500\mu m$ from the inlet in the IP calculation by using a super-relaxation factor ω of 1, 100 and 1000, respectively. While ρ approaches the steady value of $1.39kg/m^3$ in about 6×10^4 time steps with a relaxation factor ω of 1000, the evolution for $\omega=100$ is further than halfway apart from the steady state after 6×10^4 time steps, and the value of ρ remains almost the same when no super-relaxation is employed (with $\omega=1$). The maximum value of ω allowed in simulation is dependent on the smoothing technique of mass fluxes in the whole flow field: the smoother the mass flux, the larger value ω is allowed. But exaggerated smoothing would distort the flow field. A simple averaging from adjacent three points,

$$M(i,j,n)=\left(M(i-1,j,n-1)+M(i,j,n-1)+M(i+1,j,n-1)\right)/3,$$

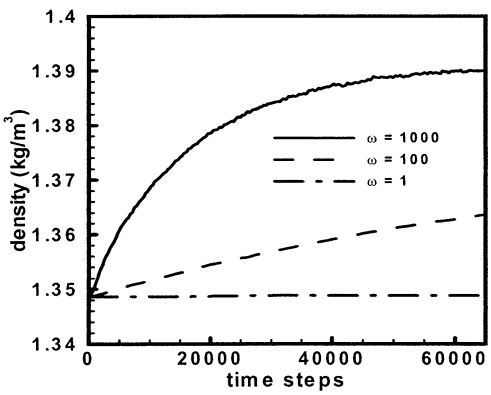

Fig. 8.13 The evolution processes of density ρ at a point located at $2500\mu m$ apart from the inlet under experimental conditions of [11] with different super-relaxation factors $\omega=1,\omega=100,\omega=1000$, respectively

where n is the number of iterations, is used. The iterated averaging for $n = 15$ has the desirable effect of smoothing, and retains the local trend of mass flux evolution. Then the value $\omega = 2000$ can be employed and the calculation remains stable. It is noted that when the steady value of ρ is being approached the value of ω and the smoothing procedure has little consequence on the final evolution result, so after having experience one can prescribe ω a varying process from say 2000 to 1 to reach the steady state, and the final result is entirely not effected by the varying process. This is satisfactory for the purpose of the calculation, for it is the final result but not the evolution process that is concerned.

In the practice of general IP method the DSMC simulated molecules move and carry the IP quantities, the DSMC process determines the IP process and the IP process has no reverse influence on the DSMC process. In the solution of channel flow and other internal flow cases, where the macroscopic quantities on the boundaries are to be regulated during the simulation, there is another specific feature, that is, the varying IP velocities on the boundaries are used to continuously adjust the boundary conditions of the DSMC–IP procedure. This influences the DSMC simulation and enables the DSMC finally to have the correct value on the boundaries. Pure DSMC process is carried out by individual molecules and the adjustment of boundary conditions is very slow and DSMC needs sufficient sample size to allow definite boundary values of $\boldsymbol{U}$ to emerge, while the IP process is a global one: the changes of IP values happen simultaneously over the whole domain of calculation and the adjustment is quick and not limited to the boundary but spreads over all the channel length. Although the approach to the steady state requires quite a long time in the example calculation under condition [11] (120 hours CPU time on a Pentium III 450, or 98.7% of the entire computation time), but during this time the global DSMC quantities are also regulated. After arriving at the steady state the sampling time required for yielding the final IP convergent data is quite short (1.6 hour CPU time, or 1.3% of the computation time).

In micro-channel experiments [10-14] the width ($40 \sim 50\mu m$) is much larger than the height ($1.2 \sim 1.33\mu m$). This made the span-wise influence negligible, and the flows can be simplified as two-dimensional (the midline velocity profile and the maximum velocity remains almost the same for rectangular cross section channels with a width to height ratio larger than 5, but the flow rate is influenced

in some minor degree by the slow down of the flow near the side wall even for large width to height ratio, see [50]). As we have seen in section 8.1, the experimental conditions [10-14] are in the slip and transition regimes.

An orthogonal coordinate system is employed with the origin located at point O, and x and y axes along OO' and OA, respectively (see Fig. 8.9). Since the flows are symmetric about OO', a computational domain of $OO'BA$ is considered only. Each of the uniform rectangular cells is sub-divided into a set of uniform rectangular sub-cells within which collision pairs are selected. The number of cells is around 400×15 to 700×30 and there are 5×2 sub-cells in each cell. The cell size is much smaller in the cross sectional direction than in the stream-wise direction, so is the sub-cell size. As shown by Nance et al. [28], the flow field is insensitive to the stream-wise cell size because of a relatively small velocity gradient in this direction. The test calculations observe that the smaller stream-wise cell and sub-cell sizes provide the same results as the present sizes being employed. For all cases the molecular interaction is described by the VHS model. The reference collision diameter in VHS appropriate to the IP method has been determined for common gases [31].

A specular reflection is used along the symmetrical boundary OO'. The channel surfaces are assumed to be diffusely reflecting with a tangential momentum accommodation coefficient σ (see Eq. (3.23)). Arkilic et al. [13, 14] developed a modified accumulation technique to measure the mass flux through micro-channels. Comparing the measured mass flow rate with the slip Navier-Stokes solution, they extracted σ for the micro-channel surfaces of single-crystal silicon in their system. The values appeared to be 0.80 ± 0.01 for argon and 0.88 ± 0.01 for nitrogen. The same means was also utilized by Shih et al. [11] to extract σ for their micro-channel surfaces, yielding 0.9905 for nitrogen and 1.1620 for helium. However, as we have seen in section 8.1, the microchannel helium flow has a Knudsen number of 0.16 at the outlet and is in the transitional regime. So extracting σ from the slip Navier-Stokes solution became improper. And the value 1.162 is beyond the physically realistic range of σ. In contrast, the nitrogen flow is in the slip regime and the value of $\sigma=0.9905$ is reasonable. This shows that the micro-channel surfaces in the UCLA system is close to the full diffuse reflection. The values of σ used in simulation for nitrogen and helium flows of [11, 12] are both 1.0 and for argon flow of [13] is 0.8 (the Knudsen

number at the exit of the argon channel flow is 0.05, and the σ value extracted from the slip Navier-Stokes solution is valid).

In the case of the channel flow of nitrogen [12] the density increment obtained by the conservative form of mass equation (8.27) and the super-relaxation method Eq. (8.28) make the mass fluxes at various sections tend to be the same (see the hollow spheres in Fig 8.11), at the same time the pressure distribution is adjusted to the actual configuration. For the inlet pressure of $19.0 psig$ the mass fluxes at various cross sections are all equal to about $4.1\times10^{-12} kg/s$. This result is in good agreement with the experimental result in [12].

Figure 8.14 compares the stream-wise pressure distributions given by the IP method with experimental data of [11] with nitrogen as the working media for the inlet pressures of 5, 10, 15, 20 and 25 $psig$, with the error bars showing the measured confidence limits. Because of the small height of $1.2\mu m$, the velocity gradient in the normal direction is quite large that leads to a strong viscous effect which is clearly demonstrated by the non-linearity of the pressure profiles. The pressure loss is subject to the local shear stress of the micro-channel surfaces that becomes sensitive to the Knudsen number as $Kn > 0.01$. For the same outlet pressure of the atmosphere, the increase of the inlet pressure results in a more significant stream-wise variation of Kn and therefore corresponds to a more obvious non-linear pressure profile. Fig. 8.15 shows the stream-wise pressure distributions at three different inlet pressures of 8.7, 13.6 and 19.0 $psig$ given by IP and

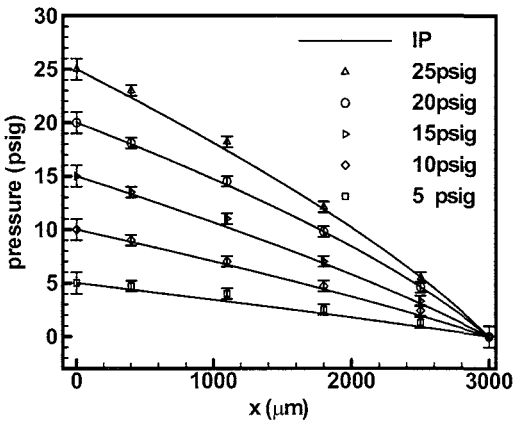

Fig. 8.14 Comparison of stream-wise pressure distributions of nitrogen flow given by IP with experimental data of [11]. $Kn_o = 0.055$ .The pressure values indicated are the inlet pressures.

experiment for helium with an exit Knudsen number of 0.16, which also agree with each other.

In Fig. 8.16 the simulated mass flux by the IP method at inlet pressures of 9.5, 15, 20, 26, 30 *psig* is compared against measured data of Shih et al. for nitrogen [12]. Fig 8.17 shows the mass flux calculated by the IP method and measured by Arkilic for argon [13]. The flows are in the slip flow regime and one can see, there is a remarkable agreement between the IP and the experimental results.

Arkilic [14] has undertaken experiments under "extreme" flow conditions to investigated flows in the transition regime. The inlet pressures of helium range from $133kPa$ to $413kPa$ (with Kn_i between 0.117 and 0.04), while the helium exhausts to a low pressure of $6.5kPa$ that results in an outlet Knudsen number of 2.5. Therefore, a significant portion of the channel lied well beyond the slip flow regime. Arkilic defined the *flow conductance* as the ratio $C = Q/\Delta p$ of mass flow to the differential pressure across the channel length and used it to check the validity of the slip Navier-Stokes model. Arkilic obtained the slope of the measured flow conductance was approximately 11% greater than the slip Navier-Stokes prediction [14] showing an obvious breakdown of the slip flow model. The data of the flow conductance has been used in [17] to check the performance of the IP method in the transitional flow regime. The value of flow conductance versus mean pressure, $\overline{P} = (P_i + P_o)/2$, given by the IP method and the experimental data of [14] , except at the largest mean pressure range, where a difference of about 5%

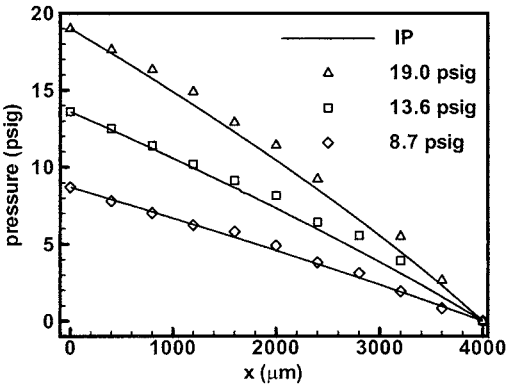

Fig. 8.15 Comparison of stream-wise pressure distributions of helium flow given by IP with experimental data of [12]. $Kn_o = 0.16$. The pressure values indicated are the inlet pressures

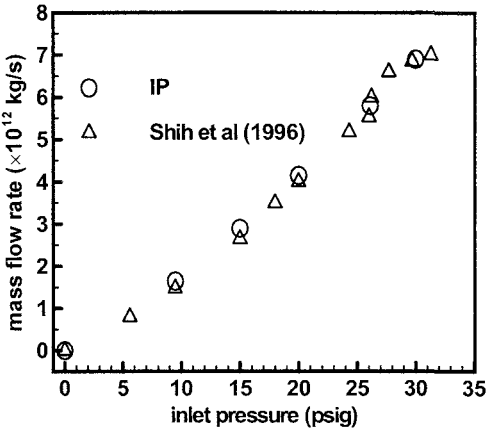

Fig. 8.16 Relation of mass flux versus the inlet pressure for the helium flow. Comparison of the IP simulation with the experimental data [12]. $Kn_o = 0.16$

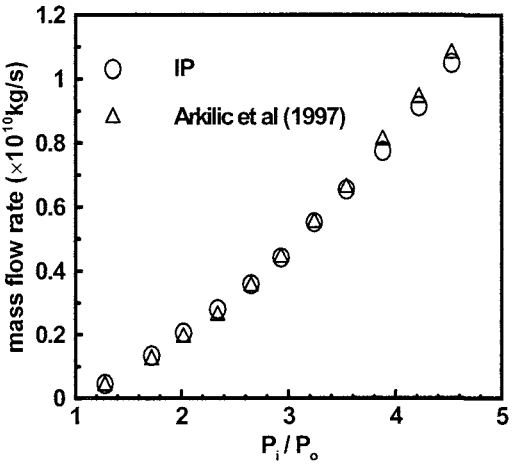

Fig. 8.17 Relation of mass flux versus the inlet pressure for the argon flow. Comparison of the IP simulation with the experimental data [13]. $Kn_o = 0.055$

appears, are generally in good agreement (see Fig.8.18). This is the first time that the result of a method appropriate for the entire transitional flow regime is compared with the experimental results of long microchannel ($1.33 \times 52.3 \times 7490 \mu m^3$) flow at rather large Knudsen numbers ($Kn_o \approx 2.5$).

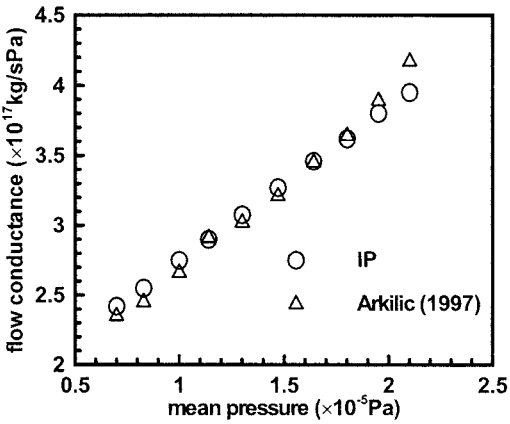

Fig. 8.18 Relation of flow conductance to mean pressure for helium flow in the transition regime. $Kn_o = 2.5$, $\sigma = 0.85$. Comparison of the IP simulation with the experimental data of [14]

8.6 THIN FILM AIR BEARING PROBLEM

The general dimensional and flow characteristics of the modern Winchester-type hard disc drive were described in section 8.1. The squeezed air bearing problem may be schematically modeled as a lower plate (the surface of the spinning platter) moving in its own plane with a velocity of U under the upper stationary tilted plate (the read/write head, see Fig. 8.19). The thin film air flow between the plates is most appropriately described by the *Reynolds equation,* which is a differential equation relating the pressure p, density ρ, platter velocity U and the height h of the gap, firstly developed by Reynolds for continuum fluid [52]. The

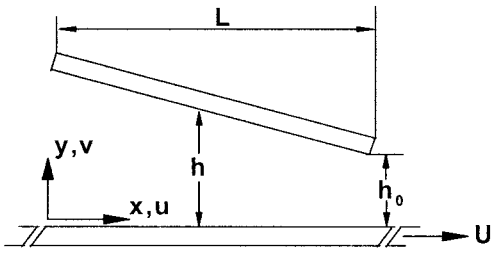

Fig. 8.19 A schematic model of the thin film air bearing flow

equation has been modified to include a number of rarefied gas dynamics effects but is still called Reynolds equation. It is essentially a mass conservation relation applied not to a fluid element but to the cross sections of the squeezed air flow and is obtained from the continuity equation by integrating it over the vertical direction with the employment of the momentum equation. Burgdorfer [53] introduced the velocity slip correction to the Reynolds equation, Fukui and Kaneko [54] developed a generalization of the equation suitable for the transitional regime.

The derivation of the Reynolds equation in the continuum regime is enlightening and can be easily extended to the slip flow and transitional flow cases so is given here. For simplicity the two-dimensional assumption is made, as the head width W is much large than the height h_o so the span wise motion can be neglected.

Writing the continuity equation

$$\frac{\partial \rho}{\partial t}+\frac{\partial \rho u}{\partial x}+\frac{\partial \rho v}{\partial y}=0 \tag{8.29}$$

in the form

$$\frac{\partial \rho v}{\partial y}=-(\frac{\partial \rho u}{\partial x}+\frac{\partial \rho}{\partial t}), \tag{8.30}$$

and integrating it over y across the whole flow region yields

$$\int_0^h d(\rho v)=-\int_0^h(\frac{\partial \rho u}{\partial x}+\frac{\partial \rho}{\partial t})dy\,. \tag{8.31}$$

The left hand side of Eq. (8.31) vanishes, as there is no fluid flown into or out of the walls. Interchanging the integration and differentiation gives

$$\frac{\partial}{\partial x}\int_0^h \rho u dy+\frac{\partial}{\partial t}(\rho h)=0\,. \tag{8.32}$$

For thin film flow with the inertial terms neglected the steady momentum Navier-Stokes equation has the form

$$\frac{\partial p}{\partial x}=\frac{\partial}{\partial y}(\mu\frac{\partial u}{\partial y})\,. \tag{8.33}$$

Integration across the gap with the non-slip boundary conditions

$$u\Big|_{y=0}=U, \quad u\Big|_{y=h}=0 \tag{8.34}$$

yields the solution of the stream wise velocity component u

$$u=U(1-\frac{y}{h})-\frac{h\partial p/\partial x}{2\mu}y(1-\frac{y}{h}). \tag{8.35}$$

Substituting Eq. (8.35) into Eq. (8.32) and accomplishing integration over y, the following equation is attained

$$\frac{\partial}{\partial x}(\frac{h^3\rho}{\mu}\frac{\partial p}{\partial x})=6\left[2\frac{\partial}{\partial t}(\rho h)+\frac{\partial}{\partial x}(\rho hU)\right]. \tag{8.36}$$

This is the general form of the Reynolds equation for the two-dimensional case. By introducing $X=x/L, H=h/h_o, P=p/p_o$ and the *bearing number*

$$\Lambda=6\mu UL/p_o h_o^{\,2}, \tag{8.37}$$

Eq. (8.36) for steady and two-dimensional case can be written in the normalized form [18]

$$\frac{d}{dX}(H^3P\frac{dP}{dX})=\Lambda\frac{d}{dX}(PH). \tag{8.38}$$

The first term of Eq. (8.35) is the slip-less solution of the velocity in the Couette flow when the upper plate is stationary and the lower plate moves towards the right with velocity U (see section 5.4.1, compare with Eq. (5.63) with $\zeta=0$), the second term is the slip-less solution of the velocity in the Poiseuille flow when the axis x is aligned along the lower plate (see section 5.4.2, the second term of Eq. (8.35) can be obtained from Eq. (5.69) by a simple translation of the ordinate y). The equation (8.38) shows that the flow rate across any cross section is the sum of the flow rate of the Couette flow and the Poiseuille flow and this rate does not change from one cross section to another in steady flow.

In section 5.4.2 we have seen that the flow rate of the Poiseuille flow with slip boundary condition surpasses that of the slip-less case by a factor

$$\frac{Q_{P,SL}}{Q_{P,C}} = (1 + 6\frac{2-\sigma}{\sigma}Kn) \tag{8.39}$$

see Eq. (5.73). As for the Couette flow the flow rates have a specific feature and are identical in slip-less case and the slip case (and even in the transitional flow case) and have the following value independent of the Knudsen number owing to the symmetry of the flow (see Fig.8.20):

$$Q_C = \rho U h / 2 . \tag{8.40}$$

From the flow rate expressions (8.39) and (8.40) for Poiseuille and Couette flows in the slip flow case one can conclude, that in the slip flow regime the following Reynolds equation is obtained in place of Eq. (8.38)

$$\frac{d}{dX}\left[(1+6\frac{2-\sigma}{\sigma}Kn)H^3 P\frac{dP}{dX}\right] = \Lambda\frac{d}{dx}(PH) , \tag{8.41}$$

where $Kn = \lambda / h$ is local Knudsen number.

When the slip boundary conditions

$$u\Big|_{y=0} = \varsigma\frac{du}{dy} , \quad u\Big|_{y=h} = -\varsigma\frac{du}{dy}, \quad \varsigma = \frac{2-\sigma}{\sigma}\lambda \tag{8.42}$$

instead of the non-slip boundary condition (8.34) is employed in solving the momentum equation (8.33), and the resulted velocity profile is substituted into the mass conservation relation (8.32), one would arrive at the same slip corrected Reynolds equation (8.41) [53, 18].

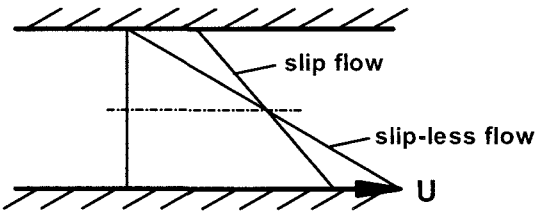

Fig. 8.20 Velocity profiles and the flow rates of the slip-less and slip Couette flow, the transitional flow is not shown but it has the same flow rate owing to the symmetry of flow

Fukui and Kaneko [19] showed that the solution of the linearized Boltzmann equation for the thin film bearing problem can be decomposed into the solutions of the plane Couette flow and the plane Poiseuille flow [55]. On this basis they derived the generalized Reynolds equation for the thin film air bearing problem by employing the flow rates of the fundamental Poiseuille and Couette flows solved by the linearized Boltzman equation. This generalized Reynolds equation in the isothermal case can be written as [19]

$$\frac{d}{dX}\left[\overline{Q}_{P,TR}(Kn)H^3P\frac{dP}{dX}\right]=\Lambda\frac{d}{dx}(PH) \tag{8.43}$$

where $\overline{Q}_{P,TR}(Kn)$ is the flow rate in transitional regime (normalized by the slip-less value $Q_{P,C}$) calculated from the linearized Boltzmann equation for Poiseuille flow and is shown to be the same as solved by Cernignani and Daneri [55]. A tabled database of the calculated values of $\overline{Q}_{P,TR}(Kn)$ for $\sigma=1$, $\sigma=0.9$, $\sigma=0.8$ and $\sigma=0.7$ is provided in [56], and a fitted formula approximation for diffuse reflection ($\sigma=1$) by Robert is recorded in [18] (there the second term on the right hand side is misprinted as $6A\sqrt{\pi}Kn$)

$$\overline{Q}_{P,TR}(Kn)=1+6AKn+\frac{12}{\pi}Kn\log(1+BKn)\,, \tag{8.44}$$

where $A=1.318889$ and $B=0.387361$. Alexander, Garcia and Alder [18] used the DSMC method to simulate the short head length air bearing problem ($L=5\mu m$, $h_o=50nm=0.05\mu m$, $U=25m/s$, $\sigma=1$), and found excellent agreement of the DSMC simulation with the generalized Reynolds equation (8.43) and Eq. (8.44). Note, their description of the latter as continuum hydrodynamic Reynolds equation corrected for slip is misleading. As we have shown, the generalized Reynolds equation is a global mass conservation relation applied to the cross section of the air bearing flow with the flow rate calculated by the Boltzmann equation which is appropriate for transitional regime. The comparison made in [18] for the cases (the ratio of the inlet to outlet heights is kept as 2:1)

$L=1.5\mu m$, $h_o=15nm=0.015\mu m$, $U=153.9m/s$, $\sigma=1.0$;

$L=5\mu m$, $h_o=50nm=0.05\mu m$, $U=25m/s$, $\sigma=0.7$;

$L = 5\mu m$, $h_o = 50nm = 0.05\mu m$, $U = 307.8m/s$, $\sigma = 1.0$;

showed good agreement of the generalized Reynolds equation with the results of DSMC simulation, this just confirms that the generalized Reynolds can be used to solve the air bearing problem in the entire transitional flow regime and can be used to test other methods intended to solve the problem, say for longer bearing head length (the authentic length of the Winchester disc drive read/write head is $\sim 1000\mu m$, but the DSMC method was able to solve only short length ($\sim 5\mu m$) problems).

The thin film air bearing problem is solved by the IP method in [57]. The rectangular area (from $x = 0$ to $x = L$, and from $y = 0$ to $y = h$ ($x = 0$)) is divided into 200×10 uniform cells for short ($L = 5 \sim 25\mu m$) length write/read head and into 1000×10 cells for long ($L = 1mm = 1000\mu m$) head. Some of them are incised by upper surface into two parts, only the one under the upper surface is within the computational domain. The cell of this part is called incomplete cell. The smallest volume of the incomplete cells is only a very small portion of that of the standard complete cell. During the process of the IP calculation, all the incomplete cells are combined with their lower adjacent complete cells. It is found that the time step is better to be kept different for the DSMC part and the IP part of the simulation process: for DSMC the usual size of the time step of the order of collision time is sufficient, but for the IP simulation a smaller time step would ensure obtaining real macroscopic quantities of the solution without much increase of the computation time. With the employment of appropriate super-relaxation factor steady convergent results can be obtained. Fig.8.21, Fig.8.22 and Fig.8.23 show the comparison of the pressure distributions for the cases of $L = 5\mu m$, $L = 25\mu m$ and $L = 1000\mu m$ of the IP results and the results of the generalized Reynolds equation. For $L = 5\mu m$ the comparison with the DSMC simulation is given as well. One can see the excellent agreement of the IP results with the generalized Reynolds equation. This can be considered as a verification of the IP method by a criterion with the merit of the strict kinetic theory. As the generalized Reynolds equation is applicable only to a certain class of problems, where as the IP method has the flexibility and the ability to treat problems with complex geometry, this

verification encourages people to use IP method to treat various complicated flow problems encountered in MEMS.

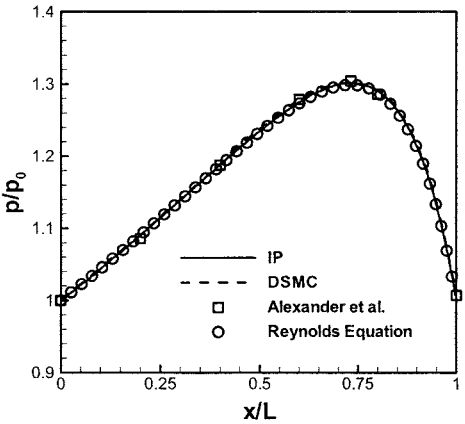

Fig. 8.21 Pressure distribution in the disc driver bearing for $Kn_o = 1.25, L = 5\mu m$, comparison of IP, DSMC and the generalized Reynolds equation results [57], also shown is the DSMC result of Alwxander et al. [18]

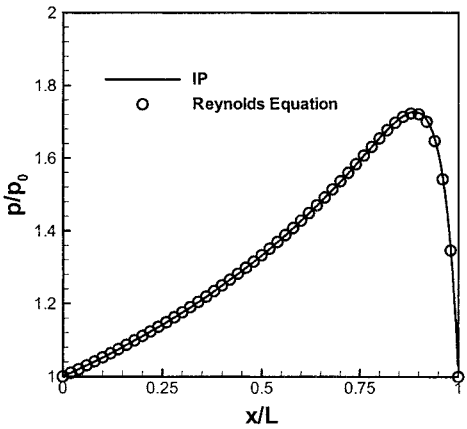

Fig. 8.22 Pressure distribution in the disc driver bearing for $Kn_o = 1.25, L = 25\mu m$, comparison of IP and the generalized Reynolds equation results [57]

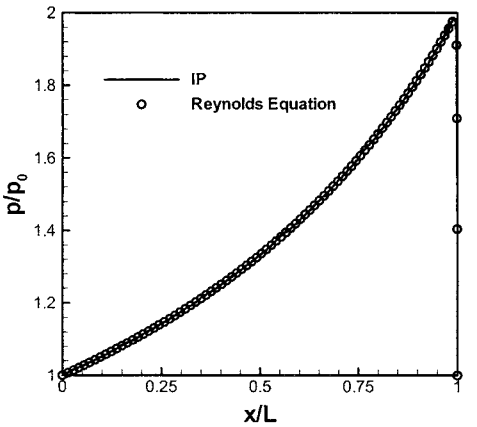

Fig. 8.23 Pressure distribution in the disc driver bearing for $Kn_o = 1.25, L = 1000\mu m$, comparison of IP and the generalized Reynolds equation results [57]

8.7 USE OF DEGENERATED REYNOLDS EQUATION IN CHANNEL FLOW

The generalized Reynolds equation (8.43) originally is derived for application in the thin film air bearing problem with the lower plate moving with a velocity U and the upper plate tilted. Shen [58] suggests degenerate this Reynolds equation and use it to solve the microchannel flow problem. In the microchannel the lower plate is stationary and the upper plate is parallel to the lower one. Owing to the steadiness of the lower plate the right hand side term vanishes, as $U = 0$ and $\Lambda = 0$, there is not any contribution of the Couette flow. Owing to the parallelity of the two plates the value H is a constant and also can be dropped from the equation. So the generalized Reynolds equation suggested for application to the microchanel problems is degenerated to the form

$$\frac{d}{dX}\left[\overline{Q}_{P,TR}(Kn)P\frac{dP}{dX}\right] = 0 . \tag{8.45}$$

The values of P on the inlet and outlet of the channel are to be specified to make the microchannel problem solvable. This degenerated Reynolds equation is

suggested be used to solve the microchannel flow in transitional flow regime provided the flow rate of the local Poiseuille flow $\overline{Q}_{P,TR}(Kn)$ in transitional regime (normalized by the slip-less value $Q_{P,C}$) is known from the strict kinetic theory. There are many works devoted to the solution of the Poiseuille flow providing the database for the flow rates at different Knudsen numbers and for different boundary conditions at the surface. With the database incorporated the degenerated Reynolds equation is valid for any surface conditions of the plates and can be integrated numerically. For example, the incomplete diffuse reflection cases with tangential accommodation coefficient $\sigma = 1$, $\sigma = 0.9$, $\sigma = 0.8$ and $\sigma = 0.7$ were calculated in [56] with tabled database of the values of $\overline{Q}_{P,TR}(Kn)$ provided under these boundary conditions. If practice has the needs, even situation with two plates having different accommodation coefficients could be considered. But for the illustrative purpose only the case of complete diffuse reflection $\sigma = 1$, is expounded here. For the case of diffuse reflection, the fitted formula approximation of $\overline{Q}_{P,TR}(Kn)$, Eq. (8.44), can be used, and the degenerated Reynolds equation attains the form

$$\frac{d}{dX}\{[1 + 6AKn + \frac{12}{\pi}Kn\log(1 + BKn)]P\frac{dP}{dX}\} = 0, \tag{8.46}$$

For the ease of integration the local Knudsen number Kn is most conveniently expressed through P, e. g., for HS model it can be written as

$$Kn = \frac{\lambda}{h} = \frac{C}{P}, \tag{8.47}$$

where

$$C = \frac{\mu}{p_0 h}\sqrt{\frac{\pi R T_0}{2}} = \lambda_0 / h = Kn_{out}, \tag{8.48}$$

for we have for hard sphere

$$\lambda = \frac{\mu}{p}\sqrt{\frac{\pi R T}{2}}, \tag{8.49}$$

see Eq. (2.222). p_0 is the pressure at the outlet, T_0 is the temperature of the gas, μ is the viscosity of the gas at T_0. The constant C has the physical

meaning of the Knudsen number at the outlet of the channel (see Eq. (8.47), at outlet $P=1$). Substituting Eq. (8.47) into Eq. (8.46), one arrives at

$$[P+6AC+\frac{12}{\pi}C\log(1+\frac{BC}{P})]\frac{dP}{dX}=D\,, \tag{8.50}$$

where D is an unspecified constant to be determined from the integration and has the physical meaning of the flow rate across the channel normalized by the slip-less flow rate value.

To illustrate the use of the degenerated Reynolds equation in solving the microchanel problem we calculate the pressure distribution for nitrogen in the $1.2\times40\times3000\mu m^3$ channel [11] and helium in the $1.2\times40\times4000\mu m$ channel [12].

For $T_0=294K$ the value of C for helium is 0.15579, and for nitrogen is 0.052325. Equation (8.50) is integrated under the following boundary condition

$$P|_{X=0}=p_{in}/p_{out}\text{ , and }P|_{X=1}=p_{out}/p_{out}=1\,, \tag{8.51}$$

with p_{in} provided by the experimental data in [11, 12]. The results of integration are presented in Fig. 8.24 and Fig. 8.25. It is seen from the figures that the results of the degenerated Reynolds equation agree well with the experimental data, and the IP simulation results have excellent agreement with those of the degenerated Reynolds equation, especially for the pressure distribution in the microchannel with dimension $1.2\times40\times4000\mu m^3$ for helium (the two curves almost coincide with each other).

In section 8.2 we have shown the unfeasibility of using LBM in simulating transitional flows in MEMS by comparison with the DSMC calculations [24, 25]. Here the LBM results [23] are compared (see [58]) with the calculations by using the degenerated Reynolds equation to attain the same conclusions as in [24, 25], but this time the conclusion is confirmed by a test stone with the merit of strict kinetic theory. Equation (8.50) is integrated under the following conditions for a short $1\times100\mu m^2$ microchannel that have been considered by LBM in Nie, Doolen and Chen [23]:

1. $C = 0.194, P\big|_{X=0} = 2, P\big|_{X=1} = 1$,

2. $C = 0.388, P\big|_{X=0} = 2, P\big|_{X=1} = 1$.

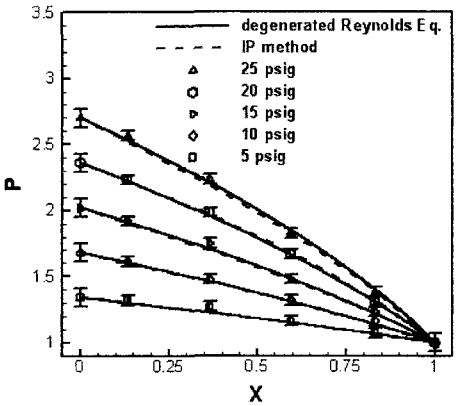

Fig. 8.24 The pressure distribution in a $1.2 \times 40 \times 3000 \mu m^3$ microchannel for nitrogen. Comparison [58] of the degenerated Reynolds equation (8.50) (solid line), the IP method (dashed line) and the experimental data [11]

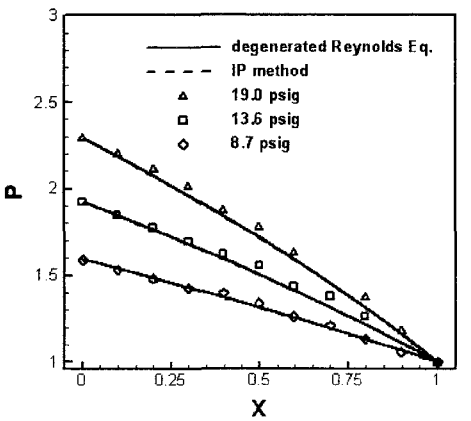

Fig. 8.25 The pressure distribution in a $1.2 \times 40 \times 4000 \mu m^3$ microchannel for helium. Comparison [58] of the degenerated Reynolds equation (8.50) (solid lines), the IP method (dashed lines, note that the solid lines and the dashed lines almost coincide) and the experimental data [12]

The results of comparison of the integration of the degenerated Reynolds equation (8.50) with the LBM, the DSMC and IP results are shown in Fig. 8.26 and Fig. 8.27. It is seen that the degenerated Reynolds equation, the DSMC method and the IP method are in excellent agreement with each other but they are in appa-

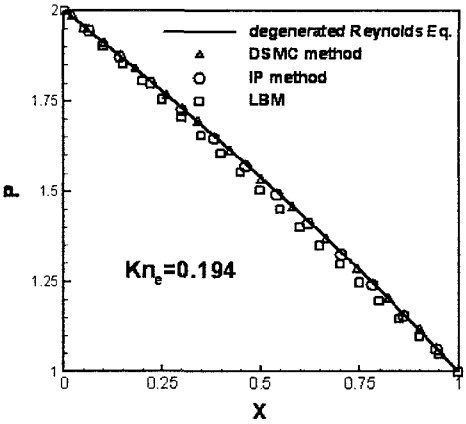

Fig. 8.26 Pressure distribution in a microchannel with $Kn = 0.194$ at outlet ($h/L = 100$). Comparison [58] of the degenerated Reynolds equation, DSMC, IP methods and the LBM method

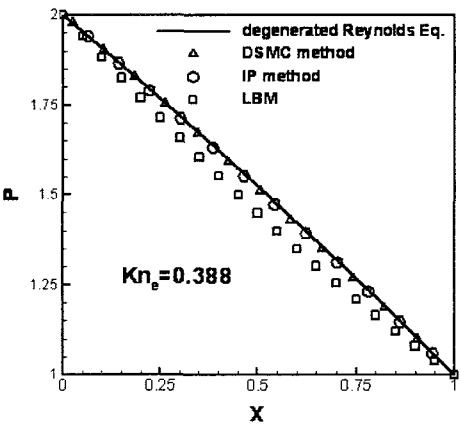

Fig. 8.27 Pressure distribution in a microchannel with $Kn = 0.388$ at outlet ($h/L = 100$). Comparison [58] of the degenerated Reynolds equation, DSMC, IP methods and the LBM method

rent disagreement with the LBM results. The LBM is shown to be unfeasible to simulate the transitional flow again, but this time by a method having the merit of kinetic theory

The generalized Reynolds equation (8.45) degenerated for application to the micro-channel problems with the flow rate $\overline{Q}_{P,TR}(Kn)$ provided by the linearized Boltzmann equation is appropriate for solving the microchannel flow problems in the entire transitional regime. It can provide the pressure distribution, the flow rate but not the detailed flow field such as the velocity profiles. But its significance lies in that it can be used as criterion of strict kinetic theoretical merit to test various methods aimed to solve the microchannel problems in transitional regime.

From the degenerated Reynolds equation (8.50) for the specific case of diffuse reflection it is seen that the microchannel rarefied gas flow is entirely specified by the inlet and outlet pressure P_{in} and P_{out}, and the Knudsen number at the outlet $C = Kn_{out}$, the length of the channel does not enter as a determining factor.

Besides the air bearing problem and the microchannel flow problem the Reynolds equation can also model the gas damping problem in micromechanical accelerometers [59]. Database for the flow rates of the Poiseuille flow with various combinations of possible surface properties calculated on the basis of linearized Boltzmann equation or other rigorous kinetic theory is desirable for the solution of microchannel flow, thin film air bearing problem and also the damping problem in the micromechanical accelerometers, especially in the form of fitting formulas.

8.8 SOME ACTUAL PROBLEMS AND CONCLUDING REMARKS

When there are temperature gradients along the MEMS or channel surfaces there occur the phenomena of thermal creep, thermal transpiration, thermal stress slip flow and the temperature stress convection etc. (see chapter 5). The Knudsen compressor in use of MEMS is worked out on the basis of thermal transpiration [60]. So it is of significance to extend the IP method to the case of temperature variation. Some useful attempt and exploration have undertaken in this aspect [32, 35, 46]. The difficulty encountered in extending the IP method to the case of temperature variation is that the average energy flux of monatomic molecules in a static gas through a surface element is $2kT\Gamma_n$, where Γ_n is the molecule num-

ber flux, but the average energy carried by a single molecule is $(3/2)kT$, the IP process can not satisfy the global energy balance across an interface. Sun [46] put forward a model of additional energy transfer and a method of assignment of the post collision IP temperature by which the IP method was able to simulate the flow between two plates with different temperatures and obtain temperature result in agreement with that of the DSMC method. But the density distribution is in some minor difference with the DSMC method. In [35] the temperature components in three directions are introduced and new method of assignment of the post collision temperature is adopted, the agreement of the temperature and density distribution with the DSMC is obtained in the flow between two plates. But these constitute only partial success for such models can not provide general method of simulation of the rarefied gas motion caused by the temperature variation. It is a challenge to modify and develop the present IP algorithm to adapt it for employment in the case of temperature variation.

The micro scale flow is usually a low speed flow as well and the flow problem is of the elliptical nature. For the external flows the size of the flow field involved in the simulation as a rule is much bigger than the body itself, thus most part of the flow field can be described by the continuum equations. For internal flows the region near the walls is described by the particle method, the region far from the walls can be described by the continuum method. The hybrid continuum/particle approach can make use of the advantages of both methods and can save enormous computation time and thus has gained extensive attention. At the interface of the continuum flow and the particle simulation boundaries (usually movable and regulated unceasingly) information must be interchanged at each time step. For ordinary particle methods owing to the huge statistical fluctuations, it is very time-consuming to pose definite boundary conditions for the continuum flow. At the same time, as the IP method preserves the macroscopic information, it is quite easy to pose boundary conditions for the continuum flow. Sun et al. [61] used hybrid IP method with the Navier-Stokes equation plus slip boundary condition to solve the flow around the plane plate and Couette flow problems and obtained smooth solutions with enhanced efficiency.

Finally, we make some concluding remarks of this chapter.

The linearized Boltzmann equation method and the DSMC method are appropriate for solving microscale rarefied gas flow problems and can be used as criteria for testing various methods intending to solve the transitional flows, the latter encounters the problem of huge statistical fluctuation for slow rarefied gas flows. The IP method preserves the averaged information of the enormous number of molecules that a simulation molecule represents, overcomes this difficulty and for low speed cases saves the computation time by a factor of $10^2 \sim 10^4$ and can treat more easily problem of complex configuration in comparison with the linearized Boltzmann equation.

The difficulty of regulating the inlet ad outlet boundary conditions of the internal flow problem is overcome by the use of conservation scheme and supper-relaxation method in the IP method. The method is validated, and on the examples of unidirectional flow, the channel flow and thin film bearing problems is checked by comparison with the experimental results, the linearized Boltzmann equation, DSMC method, the generalized Reynolds equation and the its degenerated version (with the flow rate of Poiseuille problem calculated by the Boltzmann equation). In regulating of the inlet and outlet boundary conditions the effect of super-relaxation is different from the amplification of the time interval, the requirement of sufficient small time steps remains in force to guarantee through DSMC process the true trend of the variation of the flow quantities. The super-relaxation factor amplifies the true trend and accelerates the approaching of the true solution. The regulated IP values are used as the current boundary conditions at the inlet and outlet of the DSMC process so the entire process of convergence is quickened.

The generalized Reynolds equation is appropriate to treat the thin film air bearing problem in the entire transitional regime. Example calculations and comparison with DSMC, IP and experimental results show the success of the suggestion of using the degenerated Reynolds equation to solve the transitional microchannel flow problem. Degenerated Reynolds equation with the Poiseuille flow rate calculated by the linearized Bolktzmann equation can serve as a test stone of the merit of strict kinetic theory, in particular it gives an undoubted confirmation of the unfeasibility of LBM in simulating the transitional flows. On the example of microchannel flow it provides a solid verification of the IP method.

REFERENCES

1. Knudsen M (1909) Ann Physics, 28:75
2. Millikan RA (1911) The isolation of an ion, a precision measurement of its charge, and the correction of Stokes' law. Phys Rev, 32:349
3. Millikan RA (1923) The general law of fall of a small spherical body through a gas, and its bearing upon the nature of molecular reflection from surfaces. Phys Rev, 22:1
4. Knudsen M, Weber S (1911) Ann Phys, 36:981
5. Feynman RP (1959) There's plenty of room at the bottom. Lecture on the 1959 annual meeting of AIP, in Journal of Microelectromechanical Systems, (1992) 1:60-66; also in Trimmer W (1997), Micromechanics and MEMS, Classic and Seminar Papers to 1990, Wiley, New York
6. Koplik J, Banavar J, Willemson J (1989) Molecular dynamics of fluid flow at solid surfaces. Phys. of Fluids A 1:781-794
7. Thomson P, Troian S (1997) A general boundary condition for liquid flow at solid surfaces. Nature, 389:359-362
8. Deckert KL (1990) Computer-aided design of slider bearings in magnetic disc files. IBM J Res Devel 35:660
9. Tagawa N (1993) State of the art for flying head slider mechanisms in magnetic recording disc storage. Wear 168:43
10. Liu JQ, Tai YC, Pong KC, Ho CM (1993) Micromachined channel/pressure sensor systems for micro flow studies. The 7th International Conference on Solid State Sensors and Actuators, Tranducers, 995-998
11. Pong KC, Ho CM, Liu JQ, Tai YC, (1994) Non-linear pressure distribution in uniform microchannels. ASME, FED 197, Application of Microfabrication to Fluid Mechanics, 51-56
12. Shin JC, Ho CM, Liu JQ, Tai YC, (1996) Monatomic and polyatomic gas flow through uniform microchannels. ASME-DSC 59, 197
13. Arkilic EB, Schmidt MA, Breuer KS (1997) Measurement of the TMAC in silicon microchannels, in C Shen edited Rarefied Gas Dynamics, Peking Univ. Press, 983-988
14. Arkilic EB (1997) Measurement of the mass flow and the TMAC in silicon microchannels. Ph D Thesis, MIT, DFRL TR 97-1
15. Karniadakis GE, Sherwin S (1999) Spectral/hp Element Method for CFD. Oxford Univ. Press, New York
16. Karniadakis GE, Beskok A (2001) Micro Flows, Fundamentals and Simulation. Springer-Verlag, New York, Berlin, Heidelberg
17. Shen C, Fan J, Xie C (2003) Statistical simulation of rarefied gas flows in micro-channels. J Comp Physics 189:512-526
18. Alexander FJ, Garcia AL, Alder BJ (1994) Direct simulation Monte Carlo for thin film bearings. Phys. of Fluids 6:3854-3860
19. Fukui S, Kaneko R (1988) Analysis of ultra-thin gas film lubrication based on linearized Boltzmann equation: first report-derivation of a generalized lubrication equation including thermal creep flow. J Tribology 110:253-262
20. Frish U, Hasslacher B, Pomeau Y (1986) Lattice gas automaton for the Navier-Stokes equation. *Phy. Rev Let*, 56: 1505
21. Qian Y, D'Humieres D, Lallemand P (1992) Lattice BGK models for Navier-Stokes equation. Europhysics Letters, 17:479-482

22.Chen S, Doolen GD (1998) Lattice Boltzmann method for fluid flows. Ann Rev Fluid Mech., 30:329
23.Nie X, Doolen GD, Chen S (2002) Lattice Boltzmann simulation of fluid flows in MEMS. J Stat Phys, 107:279
24.Shen C, Tian DB, Xie C, Fan J (2003) Examination of LBM in simulation of the micro-channel flow in transitional regime. Proceedings of the 1st Intern. Conference on micro and mini-channels, ASME, 405-410, see also Shen C, Tian DB, Xie C, Fan J (2004) Examination of the LBM in simulation of microchannel flow in transitional regime. Microscale Thermophysical Engineering, 8:423-432
25.Tian DB, Shen C, Xie C, Fan J (2003) The testing of the feasibility of the LBM in simulation of the transitional flow regime. Proceedings of the 2003 seminar on frontier problems of the aerodynamics (in Chinese).
26.Oran ES, Oh CK, Cybek BZ (1998) Direct simulation Monte Carlo: recent advances and applications. Ann Rev Fluid Mech 30:403
27.Oh CK, Oran ES, Sinkovits RS (1997) Computation of high-speed, high Knudsen number microchannel flows. J Thermophysics and Heat Transfer 12:447.
28.Nance RP, Hash D, Hassan HA (1997) Role of boundary conditions in Monte Carlo simulation of MEMS devices. J Thermophysics and Heat Transfer ,11:497
29.Kaplan CR, Oran ES (2002) Nonlinear filtering of low velocity gaseous micro-flows. AIAA Journal, 40:82
30.Fan J, Shen C (1999) Statistical simulation of low-speed unidirectional flows in transitional regime. Rarefied Gas Dynamics, edited by R Brun, R Campargue, R Gatignol, J C Lengrand, Cepadues Editions, 2:245-252
31.Fan J, Shen C (2001) Statistical simulation of low-speed rarefied gas flows. J Computational Physics, 167: 393-412
32.Shen C, Jiang J Z, Fan J (2001) Information preservation method for the case of temperature variation. In: T J Bartel and M A Gallis (eds) Rarefied Gas Dynamics, edited by, AIP, 585:185-192
33.Fan J, Boyd ID, Cai CP, Hennighausen K, Candler GV (2001) Computation of rarefied gas flows around a NACA 0012 airfoil. AIAA J, 39: 618-626
34.Shen C (2004) The information preservation method in simulation of internal rarefied gas flows of MEMS, invited paper, Proceedings of the 24th International Symposium on Rarefied Gas Dynamics, 11-16 July 2004, Bari, Italy, to appear in Rarefied Gas Dynamics, AIP conference proceedings
35.Jiang J Z, Shen C, Fan J (2004) Information preservation method with temperature variation, to appear
36.Sone Y, Takata S, Ohwada T (1990) Numerical analysis of the plane Couette flow of a rarefied gas. Eur J Mech., B/Fluids, 9:273
37.Gross EP, Ziering S (1958) Kinetic theory of linear shear flow. Phys. of Fluids, 1:215
38.Dong W (1956) Univ. California Report, UCRL-3353
39.Ohwada T, Sone Y, Aoki A (1989) Numerical analysis of Poiseuille flow and thermal transpiration flows. Phys. of Fluids, A1:2042
40.Gross EP, Jackson EA (1958) Kinetic theory of impulsive motion of an infinite plane. Phys. of Fluids, 1:318
41.Xie C, Fan J, Shen C (2000) Direct statistical simulation of gas flow in microchannels. Proceedings of the mass and heat transfer conference of the Chinese engineering thermophysics, p. 388 (in Chinese)

42.Cai CP, Boyd ID, Fan J, Candlir GV (2000) Direct simulation method for low speed microchannel flows. J Thermophysics Heat Transfer,14:368
43.Xie C, Fan J, Shen C (2003) Rarefied gas flows in microchannels. In: AD Ketsdever, EP Muntz edited Rarefied Gas Dynamics, AIP conference proceedings 663: 800-807
44.Sun QH, Boyd ID, Fan J (2001) Development of an IP method for subsonic, microscale gas flows. In: TJ Bartel, MA Gallis edited Rarefied Gas Dynamics, AIP conference proceedings 585: 547-553
45.Sun QH, Boyd ID, Candler GV (2001) Numrical simulation of gas flow over micro-scale airfoils, AIAA paper 2001-3071
46.Sun QH, Boyd ID (2002) A direct simulation method for subsonic, microscale gas flows. J Computational Physics, 179:400-425
47.He HG, et al (2004) Private communication
48.Fan J et al (2001) Computation of rarefied gas flows around a NACA 0012 airfoil, AIAA J, 39:618
49.Jiang JZ, Fan J, Shen C (2003) Statistical simulation of micro squire cavity flows. In: AD Ketsdever, EP Muntz edited Rarefied Gas Dynamics, AIP conference proceedings 663: 784-791
50.Jiang J, Shen C, Fan J (2003). Statistical simulation of non-circular cross section Poiseuille flows. Proceedings of the 1st Intern. Conference on micro and mini-channels, ASME, 411-418
51.Liu HL, Xie C, Shen C, Fan J (2001) Flow in membrane filter simulated as microchannel flow with diaphragm. In: TJ Bartel and MA Gallis edited Rarefied Gas Dynamics, AIP conference proceedings 585: 524-530
52.Reynolds O (1886) On the theory of lubrication and its application to Mr. Beauchamp Tower's experiments including an experimental determination of the viscosity of the olive oil. Philos Trans R Soc London, A177:157-234
53.Burgdorfer A (1959) The influence of the molecular mean free path on the performance of hydrodynamic gas lubrication bearings. Trans ASME 81:94
54.Gross WA, Matsch LA, Castelli V, Eshel A, Vohr JH, Wildman M (1980) Fluid Film Lubrication. Wiley, New York
55.Cercignani C, Daneri A (1963) Flow of a rarefied gas between two parallel plates. J Applied Physics, 34:3509-3513
56.Fukui S, Kaneko R (1990) A database for interpolation of Poiseuille flow rates for high Knudsen number lubrication problems. J Tribology 112:78-83
57.Jiang JZ, Shen C, and Fan J (2004) Statistical simulation of thin-film bearings. Paper presented at 24th international symposium on Rarefied Gas Dynamics, 10-16 July 2004, Bari, Itaty
58.Shen C, Use of the degenerated Reynolds equation in solving the microchannel flow problem, submitted to Phys. of Fluids.
59.Veijola T, Kuisma H, Lahdenpera J, Equivalent-circuit model of the squeezed gas film in a silicon accelerometer, Sensors and Actuators, A48:239 (1995)
60.Pham-van-Diep G, Keely P, Muntz EP, Weaver DP (1995) A micromechanical Knudsen compressor. In J Harvey, G Lord edited Rarefied Gas Dynamics, Oxford Univ. Press, 1:715
61.Sun QH, Boyd ID, Candler GV (2003) A hybrid continuum/particle approach for microscale gas flows. In: AD Ketsdever and EP Muntz edited Rarefied Gas Dynamics, AIP 663:752-759